Available online at www.sciencedirect.com
ScienceDirect
Catalysis Today 125 (2007) 220–228
CATALYSIS TODAY
www.elsevier.com/locate/cattod

# Effect of synergism between potassium and phosphorus on selective hydrodesulfurization performance of Co–Mo/$Al_2O_3$ FCC gasoline hydro-upgrading catalyst

Yu Fan [a,b], Jun Lu [b], Gang Shi [b], Haiyan Liu [b], Xiaojun Bao [a,b,*]

[a] State Key Laboratory of Heavy Oil Processing, China University of Petroleum, Beijing 102249, PR China
[b] The Key Laboratory of Catalysis, China National Petroleum Corp. (CNPC), China University of Petroleum, Beijing 102249, PR China

Available online 5 April 2007

**Abstract**

A series of potassium and/or phosphorus modified Co–Mo/$Al_2O_3$ FCC gasoline hydro-upgrading catalysts were prepared and the influences of potassium and/or phosphorus on the morphology, acidity and catalytic performance of the resulting catalysts were studied in the present investigation. The results showed that, compared to the single potassium or phosphorus modified catalyst, the Co–Mo–K–P/$Al_2O_3$ catalyst in which the atomic ratio of potassium to phosphorus was 2.0 could better balance the hydrodesulfurization and olefin saturation activities due to the compromised dispersion and stacking of $MoS_2$ slabs on the support as well as the good acidity property, and thus present the excellent selectivity in hydrodesulfurization. The present investigation also demonstrates the superiority of adjusting the K/P atomic ratio in optimizing the structure of $MoS_2$ slabs and thus provides a novel method for developing highly selective hydrodesulfurization catalysts.


*Keywords:* FCC gasoline; Selective hydrodesulfurization; Synergism between potassium and phosphorus; Dispersion and stacking of $MoS_2$ slabs; Acidity

## 1. Introduction

The urgent demand to reduce exhaust emissions from gasoline-powered motor vehicles makes it necessary to control the sulfur content in gasoline. More than 90% of sulfur in typical refinery gasoline pools comes from FCC gasoline [1] and thus the sulfur reduction of this stream plays an important role in clean gasoline production. It has been widely recognized that hydrotreating FCC gasoline is one of the most important deep desulfurization technologies, but the concomitant saturation of olefins in FCC gasoline gives rise to serious loss in gasoline octane number [2,3]. Therefore, selective hydrodesulfurization (HDS) that can minimize loss in gasoline octane number is highly desired to meet the severe regulations on sulfur content [4]. For this purpose, some new supports, such as $TiO_2$ [5,6], MgO [7,8] and MCM-41 molecular sieve [9], were adopted due to their good selective HDS performances. However, the relatively poor thermal stability and unsuitable mechanical properties of the above supports limited their commercial exploitation. Thus, much attention is now being paid to improving the HDS performance of conventional Co(Ni)–Mo/$Al_2O_3$ catalysts by element modification.

In view of the defects of conventional Co(Ni)–Mo/$Al_2O_3$ hydrotreating catalysts in selective HDS [10,11], Hillerova et al. [12] and Hatanaka et al. [13,14] had proposed to incorporate potassium into the catalyst supports to improve HDS selectivity, because oxide and sulfide Mo species are acidic and the alkali metal potassium modified alumina can counteract their acidity and thus enable high dispersion of the active species.

It has been widely accepted that there are two kinds of Co(Ni)–Mo–S structures: ''Co(Ni)–Mo–S(I)'', which has strong electronic interaction with support (usually γ-$Al_2O_3$), and ''Co(Ni)–Mo–S(II)'', which has weak interaction with support [15–18]. ''Co(Ni)–Mo–S(I)'' phase is ubiquitous in the conventional hydrotreating catalysts and thus its HDS activity is remarkably suppressed, as reported by Topsøe et al. [19]. It has been proven that the addition of phosphorus to alumina

* Corresponding author at: The Key Laboratory of Catalysis, China National Petroleum Corp. (CNPC), China University of Petroleum, Beijing 102249, PR China. Tel.: +86 10 89734836; fax: +86 10 89734979.
*E-mail address:* baoxj@cup.edu.cn (X. Bao).

0920-5861/$ – see front matter © 2007 Elsevier B.V. All rights reserved.
doi:10.1016/j.cattod.2007.02.022

surface not only promotes production of more polymolybdates which are easy to be sulfided [20], but also restrains the generation of Co(Ni)$Al_2O_4$ spinel which is unfavorable for forming the highly active Co(Ni)–Mo–S phase [21].

Obviously, potassium and phosphorus are promising in improving the HDS selectivity of conventional hydrotreating catalysts. However, because they were used independently in catalyst preparation, the effect of their synergism on the selective HDS performance of Co(Ni)–Mo/$Al_2O_3$ catalysts has not been touched in open literatures, to which the present investigation is addressed. Herein, the Co–Mo/$Al_2O_3$ catalyst was modified by adding single potassium, single phosphorus, and the compounds with different atomic ratios of potassium to phosphorus, and their effects on the morphology and acidity of the resulting catalysts were studied. In addition, the selective HDS performances of these catalysts were assessed with FCC gasoline as a feedstock.

## 2. Experimental

### 2.1. Catalyst preparation

Co–Mo/γ-$Al_2O_3$ catalyst was prepared by incipient wetness impregnation of γ-$Al_2O_3$ (surface area: 232 $m^2$/g, pore volume: 0.51 mL/g; Tianjin Hengmeilin Chemical Co., PR China) successively with aqueous solutions of $(NH_4)_6Mo_7O_{24}$ and $Co(NO_3)_2$ (Beijing Chemical Co., PR China) according to the required loadings. After each impregnation step, the solids were dried at 120 °C for 5 h and calcined at 520 °C for 4 h.

The catalyst modified by potassium (Co–Mo–K/γ-$Al_2O_3$) was prepared by incipient wetness impregnation of γ-$Al_2O_3$ successively with aqueous solutions of $KNO_3$ (Beijing Chemical Co., PR China), $(NH_4)_6Mo_7O_{24}$ and $Co(NO_3)_2$. Similarly, after each impregnation step, the solids were dried at 120 °C for 5 h and calcined at 520 °C for 4 h.

The Co–Mo–P/γ-$Al_2O_3$ catalyst and the Co–Mo–K–P/γ-$Al_2O_3$ catalysts with different atomic ratios of potassium to phosphorus were prepared by the same method used for preparing the Co–Mo–K/γ-$Al_2O_3$ catalyst, except for using the aqueous solutions of $H_3PO_4$, $KH_2PO_4$, $K_2HPO_4$ and $K_3PO_4$ (Beijing Chemical Co., PR China), respectively, in the first impregnation step instead of using the aqueous solution of $KNO_3$.

Table 1 lists the nomenclature of the catalysts with different compositions.

### 2.2. Catalyst characterization

The contents of Co, Mo, K and P in the catalysts were determined on a ZSX-100e X-ray fluorescence (XRF) analyzer.

The acid types of the catalysts were determined by pyridine-adsorbed Fourier transformed infrared (Py-FT-IR) spectrum experiments conducted on a Magna-IR 560 FT-IR instrument with a resolution of 1 $cm^{-1}$. Firstly, the samples were dehydrated at 500 °C for 5 h under a vacuum of $1.33 \times 10^{-3}$ Pa; then, the adsorption of purified pyridine vapor was followed at room temperature for 20 min; finally, the system was evacuated at 200 and 350 °C, and pyridine-adsorbed IR spectra were recorded.

The number and strength distributions of acid sites of the catalysts were studied by means of temperature-programmed desorption of ammonia ($NH_3$-TPD). Firstly, the samples, each 100 mg, were heated from room temperature to 600 °C at a rate of 10 °C/min and then cooled down to 100 °C in a pure He flow; then, ammonia was adsorbed at 100 °C for 20 min and subsequently the samples were purged by a flowing He stream at 100 °C for 1 h to remove excessive and physically adsorbed $NH_3$; finally, the samples were heated from 100 to 600 °C at a rate of 10 °C/min in a pure He flow and the desorption patterns were recorded. Ammonia evolved was trapped in a solution of boric acid and $NH_4Cl$, and titrated by sulfamic acid with an on-line automatic pH titrator.

X-ray photoelectron spectroscopy (XPS) analyses of the oxidic catalysts were conducted on a Shimadzu PHI-5300 ESCA spectrometer; all binding energies were calibrated using contaminant carbon ($C_{1s}$ = 284.6 eV) as a reference.

The morphologies of the active phases on the sulfided catalysts were characterized by high-resolution transmission electron microscopy (HRTEM) conducted on a Tecnai F-20 microscope (with a point-to-point resolution of 2.4 Å) equipped with a Link-ISIS-300 energy-dispersive X-ray spectrometer (EDX). The solids to be measured were ultrasonically dispersed in cyclohexane and the testing samples were prepared by dropping the dispersed suspension on carbon-coated copper grids.

### 2.3. Catalytic performance assessments

The catalytic performance assessments were carried out in a flowing-type apparatus designed for continuous operation. This apparatus consists of a gas-feeding system controlled by a mass flowmeter and a syringe pump liquid feeding system. The reactor, with an internal diameter of 10 mm, was loaded with

Table 1
Compositions of the different catalysts

| Catalyst | Designation | CoO (wt%) | $MoO_3$ (wt%) | $K_2O$ (wt%) | $P_2O_5$ (wt%) | K/P atomic ratio |
|---|---|---|---|---|---|---|
| Co–Mo/γ-$Al_2O_3$ | CM | 3.0 | 12.0 | – | – | – |
| Co–Mo–P/γ-$Al_2O_3$ | CMP | 3.0 | 12.0 | – | 4.0 | – |
| Co–Mo–K/γ-$Al_2O_3$ | CMK | 3.0 | 12.0 | 4.0 | – | – |
| Co–Mo–K–P(1[a])/γ-$Al_2O_3$ | CMKP1 | 3.0 | 12.0 | 1.6 | 2.4 | 1.0 |
| Co–Mo–K–P(2[a])/γ-$Al_2O_3$ | CMKP2 | 3.0 | 12.0 | 2.3 | 1.7 | 2.0 |
| Co–Mo–K–P(3[a])/γ-$Al_2O_3$ | CMKP3 | 3.0 | 12.0 | 2.7 | 1.3 | 3.0 |

[a] K/P atomic ratio.

the catalyst sample (ca. 4 g). The hydrocarbon compositions of the feedstock and products were determined by an Agilent 1790 gas chromatograph installed with a flame ionization detector and a HP-PONA capillary column (50 m × 0.2 mm). According to the obtained hydrocarbon compositions, the research octane numbers (RON) of the feedstock and products were calculated by a gasoline analysis software (GC 99, Beijing Research Institute of Petroleum Processing, SINOPEC, PR China). The contents of the total sulfur in the feedstock and products were measured by a WK-2C microcoulombmeter (Jiangsu Jiangfen Electroanalytical Instrument Co., PR China).

In all runs, the catalysts to be tested were brought to the identical reaction conditions. Firstly, the catalysts were presulfurized at 230 and 290 °C for 3 h, respectively, by flowing a stream containing 3 wt% $CS_2$ in cyclohexane through the catalyst bed; then, pure hydrogen gas and FCC gasoline were fed into the reactor at predetermined flow rates after the temperature was decreased to the reaction temperature; finally, the reaction was carried out under the conditions of temperature 260 °C, FCC gasoline liquid hourly space velocity (LHSV) 4 $h^{-1}$, total pressure 1.4 MPa, and volumetric ratio of $H_2$ to oil 500. After a stabilization period of 8 h, the reaction products were collected and analyzed.

The conversion of total sulfur (HDS) and the conversion of olefin hydrogenation (HYO) were calculated as follows:

$$\mathrm{HDS}(\%) = \frac{S_\mathrm{f} - S_\mathrm{p}}{S_\mathrm{f}} \times 100 \quad (1)$$

$$\mathrm{HYO}(\%) = \frac{O_\mathrm{f} - O_\mathrm{p}}{O_\mathrm{f}} \times 100 \quad (2)$$

where $S_f$ and $S_p$ indicate the mass fraction of total sulfur in the feedstock and products, respectively; $O_f$ and $O_p$ indicate the volume fraction of olefins in the feedstock and products, respectively.

The selectivity factor is defined as the ratio of the hydrodesulfurization activity to the olefin hydrogenation activity and expressed by [22]:

$$\text{selectivity factor} = \frac{(1/\sqrt[3]{S_\mathrm{p}}) - (1/\sqrt[3]{S_\mathrm{f}})}{\ln(O_\mathrm{f}/O_\mathrm{p})} \quad (3)$$

The RON loss is defined as

$$\text{RON loss} = \mathrm{RON_f} - \mathrm{RON_p} \quad (4)$$

where $RON_f$ and $RON_p$ are the RON values of the feedstock and products, respectively.

The properties of the feeding FCC gasoline are listed in Table 2.

Table 2
Properties of the feeding FCC gasoline

| | |
|---|---|
| Density (20 °C) (g $cm^{-3}$) | 0.725 |
| S (ppm) | 1140 |
| Distillation range (°C) | 32–190 |
| RON | 92.3 |
| Lumped composition (vol.%) | |
| *n*-Paraffins | 4.1 |
| *i*-Paraffins | 27.5 |
| Olefins | 40.5 |
| Naphthenes | 8.5 |
| Arenes | 19.4 |

## 3. Results and discussion

### 3.1. $NH_3$-TPD characterization

To determine the acid amount and strength of the different catalysts, $NH_3$-TPD experiments were carried out and the corresponding profiles and quantitative analysis results by the Gauss deconvolution method are presented in Fig. 1 and Table 3, respectively. From Fig. 1, we can see that there exist one or two peaks for the different catalysts: a low-temperature peak and a medium-temperature peak corresponding to the desorption of $NH_3$ from weak and medium acid sites, respectively. As shown in Table 3, the maximum desorption temperature ($T_{max1}$) for the first peak increases in the order CMK < CMKP3 < CMKP2 < CMKP1 < CMP < CM, indicating the gradual increase in acid strength [23]. It is also seen that the addition of phosphorus into Catalyst CM leads to the decrease in its acid amount of different strengths, because phosphoric acid interacts with the surface hydroxyls of alumina, resulting in the reduction in the number of hydroxyls on alumina [24,25]. Referring to the compositions of the different catalysts, one can infer that the number and strength of acid sites diminish with the increasing potassium content and the decreasing phosphorus content in the catalysts and the incorporation of potassium brings about the disappearance of medium acid sites due to its alkali property.

### 3.2. FT-IR characterization of adsorbed pyridine

In order to identify the acid type of the catalysts, the FT-IR spectra of pyridine adsorbed on the catalysts in the wavenumber range of 1600–1400 $cm^{-1}$ were measured and the results are shown in Fig. 2. The bands at 1545 and 1455 $cm^{-1}$ correspond to those specific to the pyridine molecules chemisorbed on Brönsted and Lewis acid sites, respectively [26,27], and that at 1490 $cm^{-1}$ is ascribed to the adsorbate on both Brönsted and

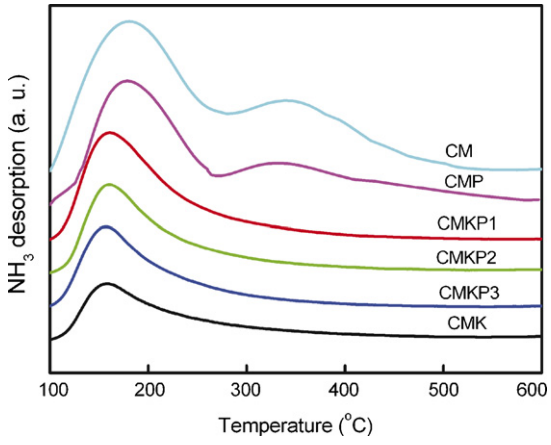


Fig. 1. $NH_3$-TPD profiles of the different catalysts.

Table 3
Acid amount and strength distributions of the different catalysts obtained by the quantitative analysis of the $NH_3$-TPD profiles shown in Fig. 1

| Catalyst | $T_{max1}$[a] (°C) | $T_{max2}$[a] (°C) | Acidity (μmol $NH_3/g_{cat}$) | | |
|---|---|---|---|---|---|
| | | | Weak acid sites | Medium acid sites | Total amount |
| CM | 182 | 340 | 293 | 224 | 517 |
| CMP | 171 | 328 | 219 | 106 | 325 |
| CMK | 151 | – | 71 | – | 71 |
| CMKP1 | 164 | – | 195 | – | 195 |
| CMKP2 | 158 | – | 151 | – | 151 |
| CMKP3 | 155 | – | 112 | – | 112 |

[a] $T_{max1}$: maximum desorption temperature for the first peak; $T_{max2}$: maximum desorption temperature for the second peak.

Lewis acid sites. Total Lewis acidity and total Brönsted acidity, and medium Lewis acidity and medium Brönsted acidity can be calculated from the spectra of pyridine adsorption at 200 and 350 °C, respectively. The quantitative analysis results by the method described elsewhere [28] are presented in Table 4.

From Fig. 2 and Table 4, it can be seen that all the catalysts have only Lewis acid sites, except that Catalyst CMP obtained by modifying Catalyst CM with single phosphorus presents weak Brönsted acid sites due to the Brönsted acidity property of phosphoric acid with three hydroxyl groups bonded to one phosphorus atom [29,30]. The results in Table 3 reveal the absence of medium acid sites in Catalysts CMKP1, CMKP2, CMKP3 and CMK, but the data in Table 4 show that there exist a small amount of medium Lewis acid sites in these potassium-containing catalysts. This difference should be attributed to the phenomenon that the medium acid sites in these potassium-containing catalysts are so few as to be concealed by the tailing of the $NH_3$ desorption peak from weak acid sites, as shown in Fig. 1. On the whole, the dependence of acid amount of different strengths on the catalyst composition shown in Table 4 is consistent with the results given in Table 3.

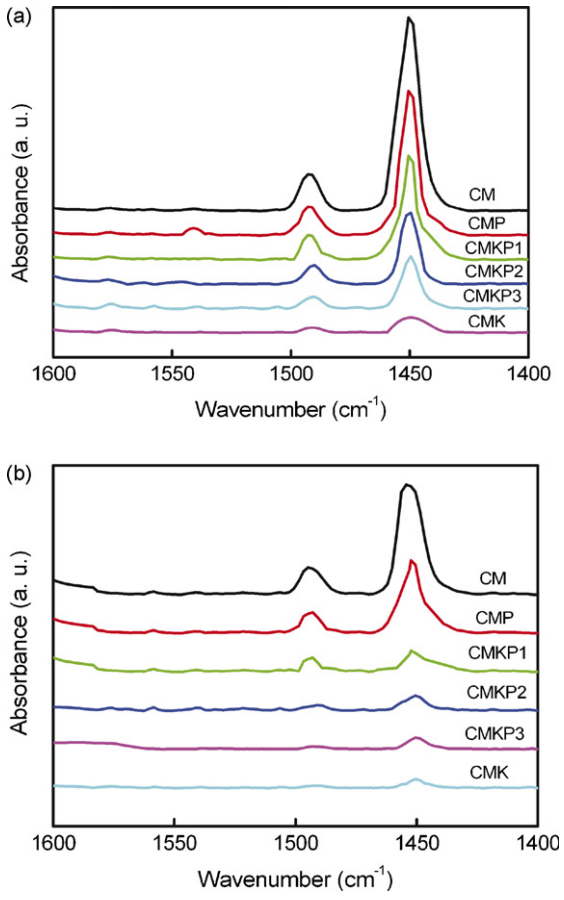


Fig. 2. FT-IR spectra of pyridine adsorbed on the different catalysts at (a) 200 °C and (b) 350 °C.

### 3.3. XPS characterization

Braun et al. [31] and Lee et al. [32] stated that the XPS intensity ratios of the metal cations in the supported metal oxide to those in the oxide support can provide the important information regarding the dispersion of the supported particles. Thus, the cobalt, molybdenum, potassium and phosphorus surface concentrations relative to aluminum in the investigated catalysts were calculated and the results are shown in Table 5. It can be seen that the Co/Al ratios on the different catalysts are identical due to the same Co content, but the Mo/Al ratios are obviously different in spite of the same Mo content on the different catalysts, indicating the different dispersion of $MoO_3$ on the different catalysts. Clearly, the dispersion of $MoO_3$ become poorer with the decreasing K/P ratio in the catalysts, suggesting that adjusting the K/P ratios can effectively control the dispersion of $MoO_3$. Because the characterization results of the oxidic catalysts, especially regarding the dispersion of the supported phases, hold for the final sulfided catalysts [33], here we can conclude that changing the K/P ratio can also tune the dispersion of $MoS_2$, as further confirmed by the HRTEM analysis results below. In addition, the different K and P

Table 4
Acid type distribution of the different catalysts obtained by the quantitative analysis of the Py-FT-IR spectra shown in Fig. 2Fig. 2

| Catalyst | Acidity (μmol/$g_{cat}$) | | | | Total amount |
|---|---|---|---|---|---|
| | Weak acid sites | | Medium acid sites | | |
| | Lewis | Brönsted | Lewis | Brönsted | |
| CM | 268.4 | – | 177.2 | – | 445.6 |
| CMP | 179.5 | 18.7 | 96.3 | – | 294.5 |
| CMK | 21.2 | – | 4.0 | – | 25.2 |
| CMKP1 | 104.3 | – | 32.8 | – | 137.1 |
| CMKP2 | 72.1 | – | 20.2 | – | 92.3 |
| CMKP3 | 31.7 | – | 9.1 | – | 40.8 |

Table 5
Surface atomic ratios on the different oxidic catalysts obtained by XPS analysis

| | Catalyst CM | Catalyst CMP | Catalyst CMK | Catalyst CMKP1 | Catalyst CMKP2 | Catalyst CMKP3 |
|---|---|---|---|---|---|---|
| Co/Al | 0.015 | 0.015 | 0.015 | 0.015 | 0.015 | 0.015 |
| Mo/Al | 0.072 | 0.021 | 0.067 | 0.034 | 0.053 | 0.059 |
| K/Al | – | – | 0.041 | 0.024 | 0.030 | 0.034 |
| P/Al | – | 0.031 | – | 0.022 | 0.018 | 0.013 |

contents in the prepared catalysts (Table 1) lead to the different K/Al and P/Al ratios in Table 5.

### 3.4. HRTEM characterization

The catalytic performance of $MoS_2$-based HDS catalysts depends on the $MoS_2$ morphology [34], so the investigation of the $MoS_2$ morphology is needed. For this purpose, high-resolution transmission electron microscopy (HRTEM), a powerful technique for studying the morphology of active phases, is usually applied. The representative HRTEM micrographs in Fig. 3 display mainly the edge or prism planes of the $MoS_2$ slabs on the different catalysts oriented along or roughly parallel to the electron beam direction. The black thread-like fringes in Fig. 3 correspond to the $MoS_2$ slabs (confirmed by EDX analysis) with about 0.6 nm interplanar distances, as pointed out by Fujikawa et al. [35].

To make a quantitative comparison of the lengths and layer numbers of the $MoS_2$ slabs on the different catalysts, statistical analyses were made based on at least ten micrographs including 300–350 slabs taken from different parts of each catalyst. The average slab length and stacking layer number were calculated according to the first moment of the distribution:

$$\frac{\sum_{i=1}^{n} n_i M_i}{\sum_{i=1}^{n} n_i} \quad (5)$$

where $M_i$ is the slab length or stacking layer number of a $MoS_2$ unit, and $n_i$ is the number of slabs or stacks in a determined range of length or stacking layer number.

The statistical results of the distribution of the $MoS_2$ slabs in length and stacking layer number are displayed in Fig. 4. It is clear that both potassium and phosphorus can increase the length and stacking layer number of $MoS_2$ slabs, but the latter is more effective.

The average layer number and length of $MoS_2$ slabs on the different catalysts are listed in Table 6. A mass of short and single-layer $MoS_2$ slabs, as presented by the single black lines in Fig. 3a, are observed on Catalyst CM due to the strong interaction between the precursor of $MoS_2$ and the alumina support [36]. From Table 6, we can see that the addition of phosphorus into Catalyst CM leads to the increases in the average slab length (from 2.08 nm on Catalyst CM to 4.34 nm on Catalyst CMP) and in the average number of layers (from 1.12 on Catalyst CM to 3.93 on Catalyst CMP) due to the increased amount of the octahedrally coordinated multilayer molybdenum species [37]. After potassium being incorporated into Catalyst CM, the nature of single-layer $MoS_2$ slabs is not changed (referring to Fig. 3c and Table 6) because of the promoting effect of potassium on the dispersion of acidic sulfide Mo species [13], but the average length of $MoS_2$ slabs increases from 2.08 nm on Catalyst CM to 2.66 nm on Catalyst CMK, indicating the relatively weaker interaction between the potassium modified support and the precursor of $MoS_2$ compared with that between the unmodified alumina support and the precursor of $MoS_2$.

Table 6
Average layer number and length of $MoS_2$ slabs on the different catalysts

| Catalyst | Average slab length (nm) | Average number of layers |
|---|---|---|
| CM | $2.08 \pm 0.03$ | $1.12 \pm 0.02$ |
| CMP | $4.34 \pm 0.07$ | $3.93 \pm 0.04$ |
| CMK | $2.66 \pm 0.04$ | $1.40 \pm 0.02$ |
| CMKP1 | $3.86 \pm 0.06$ | $3.59 \pm 0.05$ |
| CMKP2 | $3.12 \pm 0.02$ | $3.38 \pm 0.04$ |
| CMKP3 | $2.86 \pm 0.05$ | $2.11 \pm 0.03$ |

When potassium and phosphorus are simultaneously incorporated into Catalyst CM, the average length and layer number of $MoS_2$ slabs decrease with the increasing ratio of potassium to phosphorus, as shown in Fig. 3d–f and Table 6. According to Payen et al. [38], the slab length could be taken as an appropriate measure for the $MoS_2$ dispersion, so the adjustment of the K/P ratio may provide a feasible way to balance the dispersion (in accordance with the above XPS analysis results) and the stacking of $MoS_2$ slabs. The data in Table 6 show that among the three Co–Mo–K–P catalysts, Catalyst CMKP1 with the lowest K/P ratio has the longest slab length and the most layer number, suggesting the poorest dispersion and the highest stacking of $MoS_2$ slabs, while Catalyst CMKP3 with the highest K/P ratio has the least layer number and the shortest slab length, indicating the lowest stacking and the highest dispersion of $MoS_2$ slabs. Compared with the above two catalysts, Catalyst CMKP2 with a moderate K/P ratio has the well balanced dispersion and stacking of $MoS_2$ slabs, as demonstrated by its appropriate slab length and layer number in Table 6. The method to control the morphology of $MoS_2$ slabs by adjusting the K/P ratio in the catalysts, firstly reported here, sheds a light on optimizing the structure of active phases.

### 3.5. Catalytic performance assessments

Fig. 5 shows the effects of potassium and phosphorus contents in the catalysts on the olefin saturation and HDS performances. With the increasing potassium content or the decreasing phosphorus content, the HYO activity of the

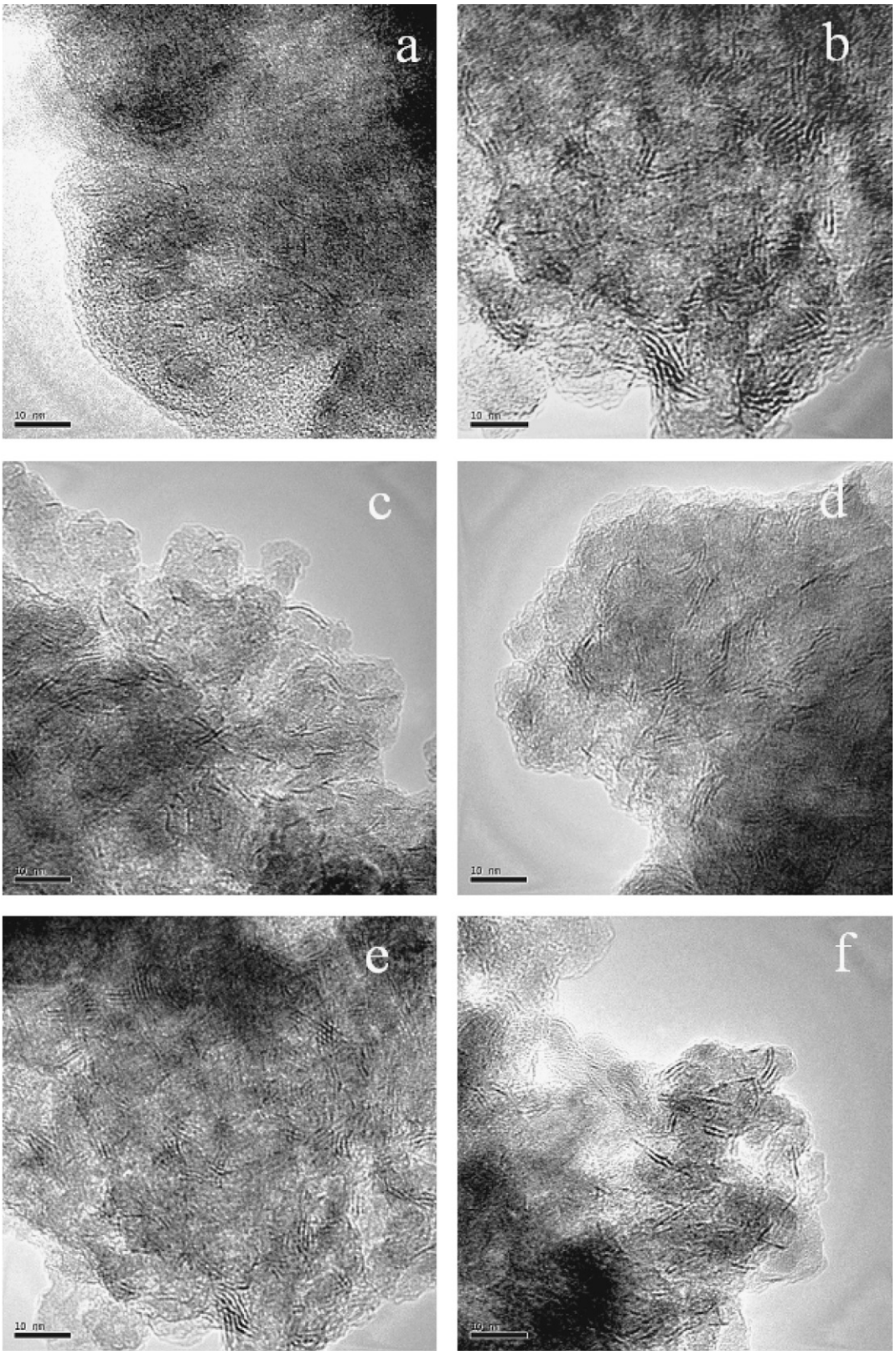


Fig. 3. HRTEM micrographs of the sulfided catalysts (a) CM; (b) CMP; (c) CMK; (d) CMKP1; (e) CMKP2; (f) CMKP3.

catalysts decreases, so does the HDS activity of the catalysts. It is obvious that the addition of potassium and phosphorus restrains the olefin saturation activity of the conventional Catalyst CM and improves its HDS performance.

Fig. 6 shows the effects of potassium and phosphorus contents in the catalysts on selectivity factor and product RON loss. It is interesting to note that increasing the potassium content or decreasing the phosphorus content in the catalysts

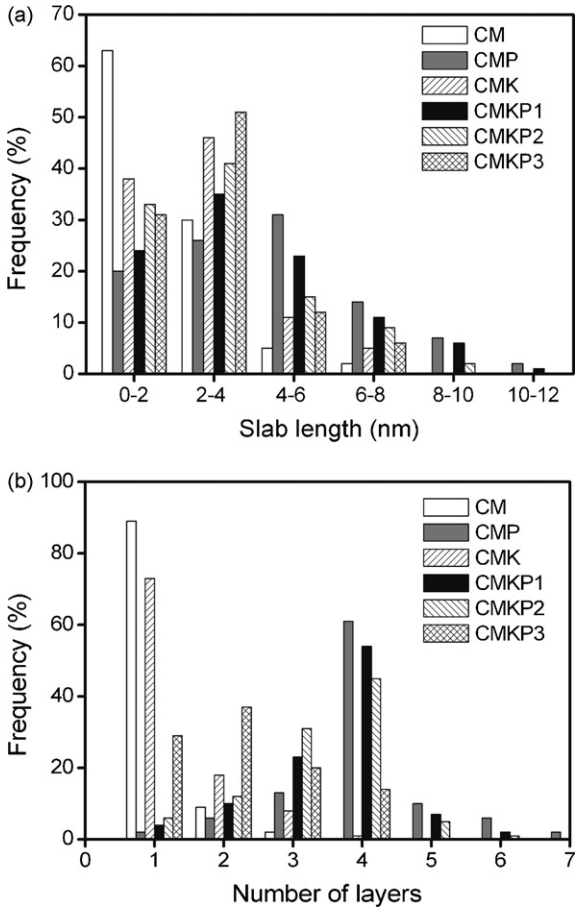


Fig. 4. Distributions of the lengths (a) and layer numbers (b) of $MoS_2$ slabs on the different catalysts.

can lessen the RON loss of the products, in coincidence with the dependence of the HYO activity of the catalysts on the potassium and phosphorus contents shown in Fig. 5. However, the selectivity factor shows a maximum with the increasing potassium content or the decreasing phosphorus content, suggesting that an optimum K/P ratio exists for achieving the

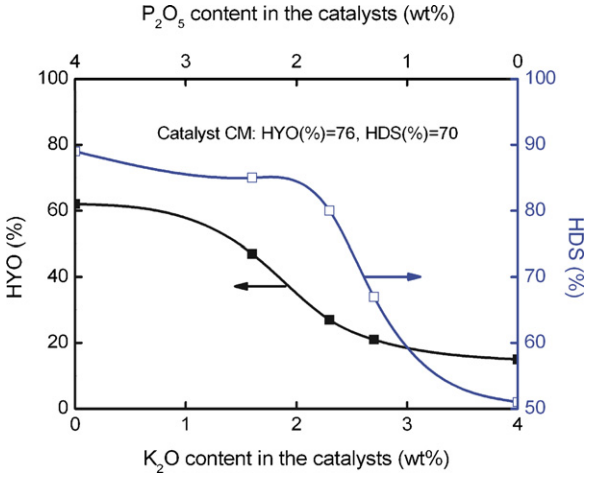


Fig. 5. Effects of potassium and phosphorus contents in the catalysts on olefin saturation and HDS performances.

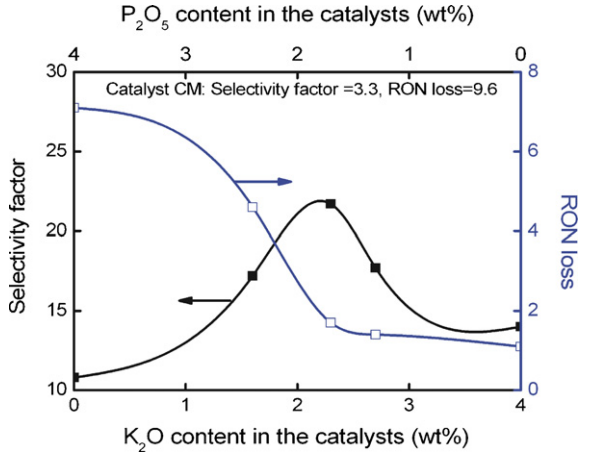


Fig. 6. Effects of potassium and phosphorus contents in the catalysts on selectivity factor and RON loss.

highest selectivity. All the catalysts modified by potassium and/or phosphorus present higher selectivity and lower RON loss than the conventional Catalyst CM.

From Figs. 5 and 6, we can conclude that from the viewpoint of all-around upgrading the product quality, the simultaneous incorporation of potassium and phosphorus is necessary. Catalyst CMKP2 with the K/P atomic ratio equal to 2.0 presents the optimum selective HDS performance, giving the HDS ratio at 80% and the RON loss at 1.7 units.

According to the rim-edge theory as discussed by Daage et al. [39,40] and Kaufmann et al. [41] (Fig. 7), the rim sites of a $MoS_2$ slab can catalyze both HDS and HYO reactions, but the edge sites can only catalyze the HDS reaction. By considering the relationship between the different morphologies of the catalysts and their catalytic performances, we notice the following facts: the addition of phosphorus into Catalyst CM decreases the catalyst acidities of different strengths (Tables 3 and 4) and greatly increases the stacking degree of the active species $MoS_2$ slabs (Table 6) due to the weakened interaction between the active species and the alumina support [24,37], so more edge sites that are favorable for improving the catalyst HDS activity are formed and the number and acidity of the rim sites are reduced. As a result, the HDS activity of Catalyst CMP is higher than that of Catalyst CM and the HYO activity of the former is lower than that of the latter. However, compared with the other four catalysts, Catalyst CMP has higher HYO activity because of its more acid sites with different strengths (Fig. 5 and Table 3).

As shown in Figs. 3a and c, the addition of potassium into Catalyst CM does not significantly change its single-layer dispersion nature of $MoS_2$ slabs, so the resulting catalyst still has abundant rim sites. Nevertheless, the acidity of these rim sites is considerably decreased due to the neutralization effect of alkali metal potassium on acidic sulfide Mo species [13]. It is the decreased acidity of the rim sites that causes the reduction in both HYO and HDS activities of Catalyst CMK, in accordance with the results reported by Leyrit et al. [42].

When potassium and phosphorus are simultaneously incorporated into Catalyst CM, we find that the K/P ratio

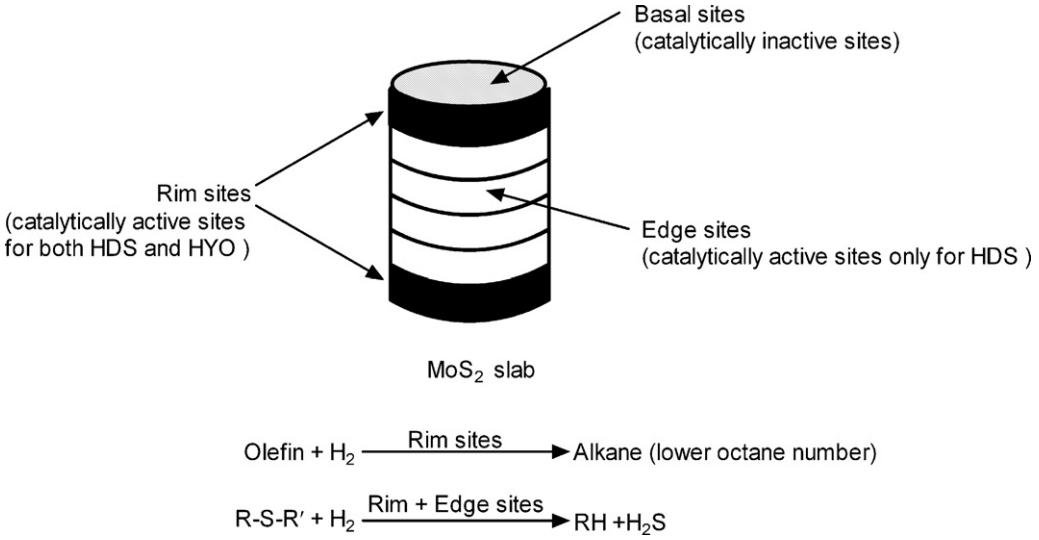


Fig. 7. Catalytically active sites on $MoS_2$-based HDS catalysts.

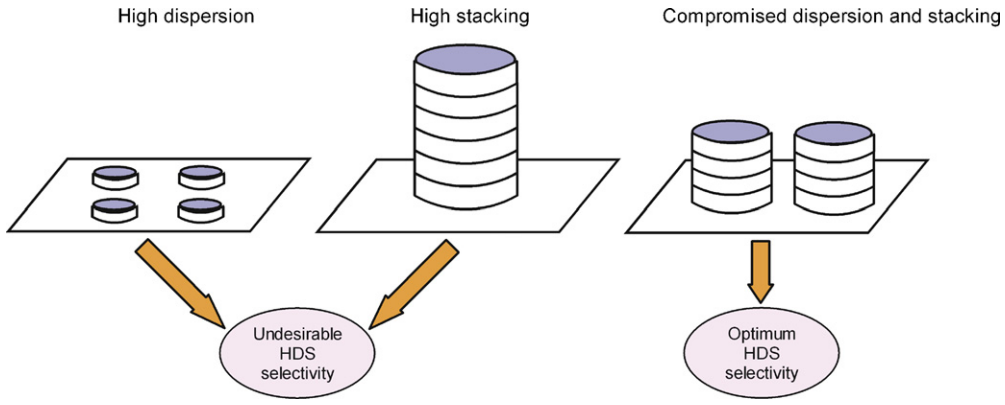


Fig. 8. Schematic representation for optimizing the dispersion and the stacking of $MoS_2$ slabs.

can significantly impact the HDS selectivity of the resulting catalysts. Although the higher stacking structure of $MoS_2$ slabs on Catalyst CMKP1 with the low K/P ratio can promote the formation of Co–Mo–S (II) phase due to the weak interaction between the active species and the support, the difficult accessibility of active sites on the catalyst surface as a result of the lower dispersion leads to the undesirable selective HDS activity (Table 6 and Fig. 6). On the other hand, the highly dispersed $MoS_2$ slabs on Catalyst CMKP3 with the high K/P ratio cannot meet the requirement of high selectivity due to the competitive adsorption of sulfur compounds and olefins on the only active sites, namely the rim sites (Table 6 and Fig. 6). It is the balanced dispersion and stacking of $MoS_2$ slabs on Catalyst CMKP2 with the appropriate K/P ratio that guarantees the optimum HDS selectivity.

The above results confirm that the high dispersion of $MoS_2$ slabs cannot ensure the excellent catalyst HDS selectivity, nor can the high stacking of $MoS_2$ slabs. To achieve the best HDS selectivity, a compromise between the dispersion and the stacking of $MoS_2$ slabs is critical, as schematically depicted in Fig. 8.

## 4. Conclusions

To improve the selective hydrodesulfurization (HDS) performance of the conventional Co–Mo/$Al_2O_3$ FCC gasoline hydro-upgrading catalyst, potassium and/or phosphorus modifications were introduced and a novel method by adjusting the atomic ratio of potassium to phosphorus in the catalysts was proposed.

The results showed that the addition of phosphorus greatly increased the stacking degree of $MoS_2$ slabs on the conventional catalyst and therefore enhanced its HDS activity. However, the excessive acid sites in the phosphorus modified catalyst led to the massive saturation of olefins and thus gave rise to a serious loss in gasoline octane number.

Compared with the phosphorus modified catalyst, the potassium modified catalyst presented poor HDS activity because of the excessive decrease in the catalyst acidity, despite the great depression in olefin hydrogenation activity due to the neutralization effect of alkali metal potassium on acid sites of the conventional catalyst.

Different from the above two catalysts, the Co–Mo–K–P/$Al_2O_3$ catalyst with a suitable atomic ratio of potassium to

phosphorus had the well balanced HDS and olefin hydrogenation activities due to the compromised dispersion and stacking of $MoS_2$ slabs on the support as well as the good acidity property, and thus greatly improved the quality of the upgraded FCC gasoline.

The finding obtained in the present investigation may shed a light for developing highly selective HDS catalysts.

## Acknowledgements

This work was supported by the National Basic Research Program of China (Grant No. 2004CB217807), the Natural Science Foundation of China (Grant No. 20606037), and the CNPC Innovation Foundation (Grant No. 05E7020).

## References

[1] S. Brunet, D. Mey, G. Pérot, C. Bouchy, F. Diehl, Appl. Catal. A: Gen. 278 (2005) 143.
[2] T. Klimova, D.S. Casados, J. Ramírez, Catal. Today 43 (1998) 135.
[3] M. Toba, Y. Miki, Y. Kanda, T. Matsui, M. Harada, Y. Yoshimura, Catal. Today 104 (2005) 64.
[4] D. Solis, T. Klimova, J. Ramírez, T. Cortez, Catal. Today 98 (2004) 99.
[5] S. Srinivasan, A.K. Datye, C.H.F. Peden, J. Catal. 137 (1992) 513.
[6] A.K. Datye, S. Srinivasan, L.F. Allard, C.H.F. Peden, J.R. Brenner, L.T. Thompson, J. Catal. 158 (1996) 204.
[7] T. Klicpera, M. Zdrazil, J. Catal. 206 (2002) 314.
[8] J. Cinibulk, P.J. Kooyman, Z. Vit, M. Zdrazil, Catal. Lett. 89 (2003) 147.
[9] C. Bai, G.B. McVicker, S.S. Shih, M.C. Kerby, E.A. Lemon J.R., US Patent 0,049,083A1 (2006).
[10] S. Hatanaka, M. Yamada, O. Sadakane, Ind. Eng. Chem. Res. 36 (1997) 5110.
[11] S. Hatanaka, M. Yamada, O. Sadakane, Ind. Eng. Chem. Res. 37 (1998) 1748.
[12] E. Hillerova, Z. Vir, M. Zdrazil, Appl. Catal. 118 (1994) 111.
[13] S. Hatanaka, T. Miyama, H. Seki, S. Hikita, EP Patent 0,736,589 (1996).
[14] S. Hatanaka, O. Sadakane, S. Hikita, T. Miyama, US Patent 5,853,570 (1998).
[15] H. Topsøe, B.S. Clausen, Catal. Rev. Sci. Eng. 26 (1984) 395.
[16] V.M. Brown, S.P.A. Louwers, R. Prins, Catal. Today 10 (1991) 345.
[17] S.P.A. Louwers, M.W.J. Craje, A.M. van der Kraan, C. Geantet, R. Prins, J. Catal. 144 (1993) 579.
[18] S. Eijsbouts, Appl. Catal. A: Gen. 158 (1997) 53.
[19] H. Topsøe, B.S. Clausen, F.E. Massoth, Hydrotreating Catalysis—Science and Technology, Springer-Verlag, Berlin, 1996.
[20] S.I. Kim, S.I. Woo, J. Catal. 133 (1992) 124.
[21] P. Atanasova, T. Halachev, Appl. Catal. 48 (1989) 295.
[22] M.P. Lapinski, K.L. Riley, T.R. Halbert, W. Lasko, J.L. Kaufman, US Patent 6,126,814 (2000).
[23] F. Arena, R. Dario, A. Parmaliana, Appl. Catal. A: Gen. 170 (1998) 127.
[24] A. Morales, M.M. Ramírez de Agudelo, F. Hernández, Appl. Catal. 41 (1988) 261.
[25] A. Stanislaus, M. Absi-Halabi, K. Al-Dolama, Appl. Catal. 39 (1988) 239.
[26] G. Busca, Catal. Today 41 (1998) 191.
[27] J.A.Z. Pieterse, S. Veefkind-Reyes, K. Seshan, L. Domokos, J.A. Lercher, J. Catal. 187 (1999) 518.
[28] Y. Fan, D. Lei, G. Shi, X.J. Bao, Catal. Today 114 (2006) 388.
[29] C.W. Fitz Jr., H.F. Rase, Ind. Eng. Chem. Res. 22 (1983) 40.
[30] R. Lopez Cordero, N. Esquivel, J. Lazaro, J.L.G. Fierro, A. Lopez Agudo, Appl. Catal. 48 (1989) 341.
[31] S. Braun, L.G. Appel, V.L. Camorim, M. Schmal, J. Phys. Chem. B 104 (2000) 6584.
[32] J.J. Lee, H. Kim, J.H. Koh, A. Jo, S.H. Moon, Appl. Catal. B: Environ. 58 (2005) 89.
[33] S. Dzwigaj, C. Louis, M. Breysse, M. Cattenot, V. Bellière, C. Geantet, M. Vrinat, P. Blanchard, E. Payen, S. Inoue, H. Kudo, Y. Yoshimura, Appl. Catal. B: Environ. 41 (2003) 181.
[34] H. Shimada, Catal. Today 86 (2003) 17.
[35] T. Fujikawa, H. Kimura, K. Kiriyama, K. Hagiwara, Catal. Today 111 (2006) 188.
[36] J.V. Lauritsen, S. Helveg, E. Lægsgaard, I. Stensgaard, B.S. Clausen, H. Topsøe, F. Besenbacher, J. Catal. 197 (2001) 1.
[37] S.M.A.M. Bouwens, A.M. van der Kraan, V.H.J. de Beer, R. Prins, J. Catal. 128 (1991) 559.
[38] E. Payen, R. Hubaut, S. Kasztelan, O. Poulet, J. Grimblot, J. Catal. 123 (1994) 147.
[39] M. Daage, R.R. Chianelli, A.F. Ruppert, Stud. Surf. Sci. Catal. 75 (1993) 571.
[40] M. Daage, R.R. Chianelli, J. Catal. 149 (1994) 414.
[41] T.G. Kaufmann, A. Kaldor, G.F. Stuntz, M.C. Kerby, L.L. Ansell, Catal. Today 62 (2000) 77.
[42] P. Leyrit, T. Cseri, N. Marchal, J. Lynch, S. Kasztelan, Catal. Today 65 (2001) 249.